POLİTEKNİK DERGİSİ

JOURNAL of POLYTECHNIC

ISSN: 1302-0900 (PRINT), ISSN: 2147-9429 (ONLINE)
URL: http://dergipark.org.tr/politeknik

Stabilization of two axis gimbal system with self tuning pıd control

Kendinden ayarlamalı pid denetleyici ile iki eksenli gimbal sisteminin stabilizasyonu

***Yazar (Author)**: Murat ŞAHİN[1]*

ORCID[1]: 0000-0002-3659-3528

To cite to this article: Sahin M., "Stabilization of two axis gimbal system with self tuning pıd control", ***Journal of Polytechnic***, 27(4): 1441-1452, (2024).

Bu makaleye şu şekilde atıfta bulunabilirsiniz: Sahin M., "Stabilization of two axis gimbal system with self tuning pıd control", ***Politeknik Dergisi***, 27(4): 1441-1452, (2024).

Erişim linki (To link to this article): http://dergipark.org.tr/politeknik/archive

DOI: 10.2339/politeknik.1210906

Stabilization of Two Axis Gimbal System with Self Tuning PID Control

Highlights

- *Gimbal systems have problems such as unbalanced, cross-coupling, and unmeasurable distortions.*
- *Fuzzy-based control is straightforward and independent of the model.*
- *Basic PID principles are used when creating rule tables.*
- *Choosing the most appropriate coefficient at every step.*
- *Self-tuning method increases the robustness of the controller.*

Graphical Abstract

This study carried out controller design and implementation studies within the scope of stabilization of a two-axis gimbal system used in the missile. With the STF-PID, the PID coefficients were adjusted differently at each step, and a more efficient controller was obtained.

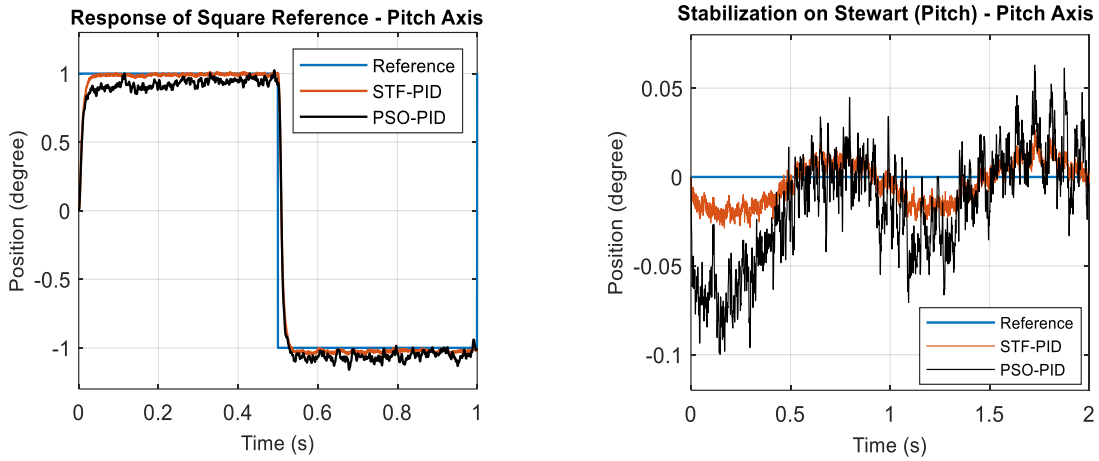

Figure. Test results

Aim

Stabilization of a two-axis gimbal system used in the missile.

Design & Methodology

Self-Tuning PID controller based on Fuzzy Logic.

Originality

Original work has been done for the gimbal system and has not been published elsewhere.

Findings

The stabilization errors of 20E-3 degrees were reached with STF-PID. Error values exceeded 50E-3 degrees with the classical PID.

Conclusion

The adjustable PID controller is more suitable than the fixed coefficient PID controller for the gimbal with uncertainties.

Declaration of Ethical Standards

The author of this article declare that the materials and methods used in this study do not require ethical committee permission and/or legal-special permission.

Stabilization of Two Axis Gimbal System with Self Tuning PID Control

Research Article

Murat ŞAHİN*

Control Systems Department, Roketsan A. S., 06780 - Elmadag, Ankara, Türkiye

(Received : 28.11.2022 ; Accepted : 26.06.2023 ; Early View : 03.09.2023)

ABSTRACT

Gimbal is a system that provides locking and tracking of the seeker on the target in missiles and increases the angle of view with its mobility in two axes. In this study, stabilization of a two-axis gimbal system used in the missile was carried out. In gimbal stabilization, adaptive controllers are preferred instead of classical controllers due to unbalance, cross-coupling, and unmeasurable disturbances. A Self Tuning PID controller based on Fuzzy Logic was developed for axis controls in the stabilization algorithm. Thanks to this controller, which works with the principle of choosing the most appropriate coefficient at every step, it was possible to control with less than 3% errors in the tests performed with the flight simulator. In addition, a PID controller whose coefficients are optimized with Particle Swarm Optimization is designed for comparison purposes. In experimental studies, it was seen that PID with adjustable coefficients gave better results than the fixed PID.

Keywords: Gimbal, fuzzy logic, self-tuning controller, PID, particle swarm optimization

Kendinden Ayarlamalı PID Denetleyici ile İki Eksenli Gimbal Sisteminin Stabilizasyonu

ÖZ

Gimbal, füzelerde arayıcının hedef üzerinde kilitlenmesini ve takibini sağlayan, iki eksende hareket kabiliyeti ile görüş açısını arttıran bir sistemdir. Bu çalışmada, füzede kullanılan iki eksenli bir gimbal sisteminin stabilizasyonu gerçekleştirilmiştir. Gimbal stabilizasyonunda dengesizlik, çapraz kuplaj ve ölçülemeyen bozucu etkenler nedeniyle klasik denetleyiciler yerine uyarlamalı denetleyiciler tercih edilmektedir. Stabilizasyon algoritmasındaki eksen kontrolleri için Bulanık Mantık tabanlı Kendinden Ayarlamalı PID denetleyici geliştirilmiştir. Her adımda en uygun katsayının seçilmesi prensibi ile çalışan bu denetleyici sayesinde, uçuş simülatörü ile yapılan testlerde %3'ten daha az hata ile stabilizasyon gerçekleştirmek mümkün olmuştur. Ayrıca karşılaştırma amacıyla Parçacık Sürü Optimizasyonu ile katsayıları ayarlanmış bir PID denetleyici tasarlanmıştır. Deneysel çalışmalarda katsayıları kendinden ayarlanabilir PID denetleyicinin, sabit PID denetleyiciye göre daha iyi sonuç verdiği görülmüştür.

Anahtar Kelimeler: Gimbal, bulanık mantık, kendinden ayarlamalı denetleyici, PID, parçacık sürüsü optimizasyonu.

1. INTRODUCTION

Gimbal systems stabilize sensors such as cameras, radars, lasers, and similar platforms. The sensor system is protected from external disturbances thanks to stabilization, and more sensitive measurements can be made [1]. Due to these features, it has been widely used in unmanned aerial vehicles, missiles, and robots in recent years. Stabilization can be done with a single axis to control vertical movement relative to the base for some applications [2]. However, it is usually provided by more than one axes in platforms. UAVs and mini-missiles have volumetric constraints. This situation has made 2-axis designs more common due to fewer mechanical parts [3]. The axes of the two-axis gimbal are orthogonal to each other and have free movement capability. The camera or sensor system is located on the inner axis. Each axis is controlled by separate actuators, providing the torque and movement required for stabilization [4]. Two methods are generally used for line of sight (LOS) stabilization. The angular velocity sensor (AVS) is mounted on the LOS axis in the first method, thereby increasing accuracy by direct measurement. In the second method, AVS is mounted on the system's base where the gimbal is placed. This method is called indirect LOS stabilization, and stabilization error may occur due to unmeasurable distortions in the LOS framework [5]. In this study, the AVS is mounted on the LOS axis.

One of the problems frequently encountered in gimbal systems is the unbalance problem. This problem is caused by the shift of the center of gravity due to mechanical design/manufacturing, material, and assembly errors [6]. Another critical issue is cross-coupling. The movement of one axis naturally affects the other axis. When these movements are at high speeds, they can cause vibrations on different axes [7]. Unmeasurable distortions and model uncertainties in the

*Sorumlu Yazar (Corresponding Author)
e-posta : msahin@roketsan.com.tr

LOS framework also pose problems [8]. The LOS needs to be stabilized sensitively to external factors for accurate tracking. Robust control methods are necessary because of both uncertainties of the gimbal model and the disturbances [9]. There are many different types of control design studies in the literature. Studies with sliding mode control (SMC) stand out for their fast response times and high robustness against external disturbances. During the control with classical SMC, sudden stops may occur due to saturation in the actuators and then sudden accelerations again. This situation also directly affects the stabilization. Proxy-based SMC has been proposed to dampen these harsh movements. Due to the discontinuity in the signum function, it is challenging to perform the SMC in discrete time. It can cause time delays in components such as sensors and actuators. In order to prevent this time delay, a virtual proxy object is added to the control loop [10]. There is also the threat of the chattering phenomenon in traditional SMC. One of the efforts to eliminate this threat is Fractional Order SMC. These studies add more design parameters and look at the older history of the input signals. This way, the sliding surfaces and the control torques can be matched more precisely. It is also made adaptive by combining with Lyapunov-based structures [11, 12]. These studies make the model more complex. In order to work on a simpler model, a continuous finite-time SMC with a step control structure is proposed. This structure can predict without advanced model and calibration data. It is tried to reduce chattering by controlling the current with FOC in the cascade structure [13]. Sensor noise is another problem that complicates the control of the gimbal system despite detailed modeling and calibration studies. Because high-resolution gyro sensors are also sensitive to noise, feedback is also noisy. In such cases, one of the effective control methods is the H∞ method. The H∞ method evaluates the control error, the amplitude of the controller signal, and the ideal system output to be achieved and performs an optimization. Thus, it tries to produce the best control signal at each step [14, 15]. Model predictive control has also been proposed as part of gimbal stabilization. However, due to the reasons mentioned above, the gimbal contains uncertainties, so it is challenging to prepare an accurate model, and it is recommended to include nonlinear factors. Altan and Hacioglu used the Hammerstein model, which is used to identify nonlinear systems while preparing the gimbal model in their study. [16]. Another method is the Fuzzy Logic (FL) method. The adaptability of the FL for systems with nonlinear and uncertain factors has also made it preferred for gimbal systems [17, 18]. Besides robust controllers, PID controllers are also used because of their simplicity and flexibility [19]. However, adaptive PID controllers are used instead of classical PID due to non-modelable factors such as vibration, resonance, and friction [20]. It is also seen that PID controllers are combined with FL to increase their robustness. Instead of fixed PID coefficients, online coefficient tuning was performed with FL and tested on gimbal stabilizations [21, 22].

This study carried out studies within the scope of stabilization of the gimbal used in a missile. In similar studies, robust control methods are used due to unbalance problems, model uncertainties, and unpredictable external noises. In model-based applications, even when modeling with nonlinear methods, it is also used with adaptive methods due to uncertain situations. In fuzzy-based studies, the control method is more straightforward and model-independent. In this study, a fuzzy-based self-tuning PID control method has been developed by utilizing the ability of the fuzzy to adapt quickly to variable conditions. As in some SMC studies, the error derivative was used in addition to the error. In this way, the change of the error was added to the control method. The gimbal used in the study has a mechatronic structure, and DC motors control its axes. The equations and models of gimbal dynamics are included in the second part of the study. In the third part, there are stabilization algorithms design studies. In order to compare the fuzzy-based self-tuning PID controller, a PID controller whose coefficients are calculated by the Particle Swarm Optimization (PSO) method has also been developed. In the last section, there are experimental studies and evaluations.

2. DYNAMIC MODEL OF GIMBAL SYSTEM

Gimbal consists of two axes. The outer axis is the yaw axis, and the inner axis is the pitch axis. The camera and the gyro sensor, which can measure in two axes, are on the inner axis. The general view of the gimbal is given in Figure 1 [23].

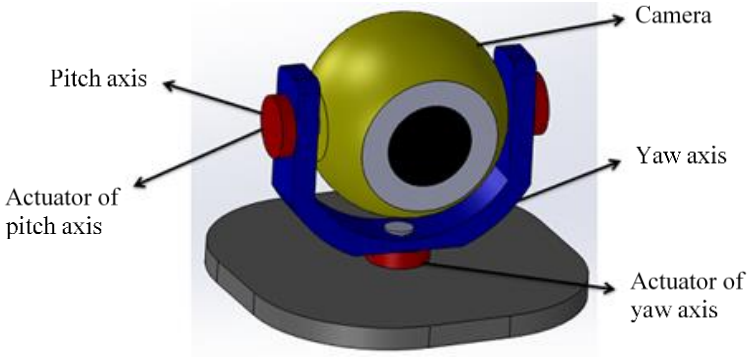

Figure 1. The general view of the gimbal system

Dynamic equations need to be defined when modeling the gimbal. The dynamics are calculated from the relationship between the torque produced by the system and the axis movements and can be defined by the Lagrange Equation [24]. Motion representations are given in Figure 2.

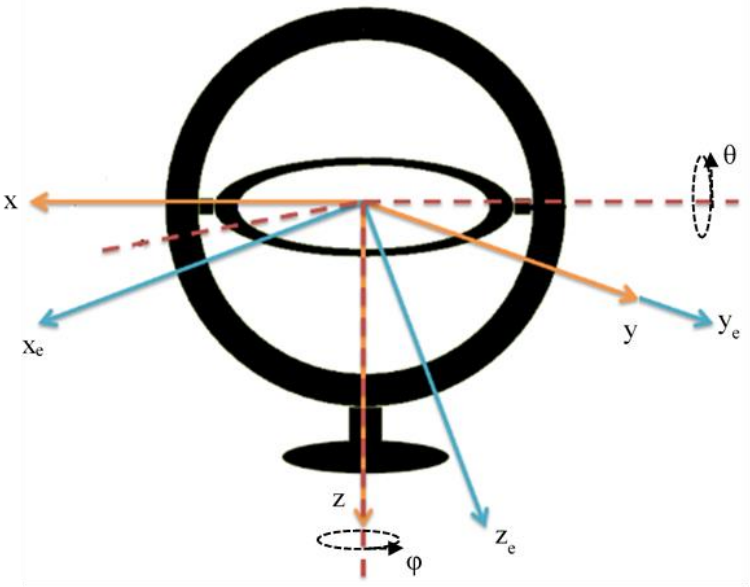

Figure 2. Movement of the gimbal system

The Lagrangian equation is an energy equation and uses kinetic and potential energy. The equations indicate the inner gimbal wring as I, the outer gimbal wring as D, and the camera as K. The total kinetic energy (KE) will equal the sum of the kinetic energies of I, D, and K [10].

$$KE = \frac{1}{2}\left[(J_{Ky} + J_{Iy})\dot{\theta}^2 + (J_{Kx} + J_{Ix})\dot{\varphi}^2\, sin^2(\theta) + (J_{Kz} + J_{Iz})\dot{\varphi}^2\, cos^2(\theta) + (J_{Dz})\dot{\varphi}^2\right] \quad (1)$$

In equation (1), J_K represents the camera inertia matrix, J_I is the inner gimbal wring inertia matrix, J_D is the outer gimbal wring inertia matrix. $\dot{\theta}$ indicates the angular velocity about the horizontal pitch axis, θ the vertical axis rotation, $\dot{\varphi}$ the angular velocity about the vertical yaw axis, and φ the yaw axis rotation. The potential energy equation is also denoted by (2) [10]. Here, m denotes the total mass of the camera, and inner gimbal wring, and l denotes misalignment. (As can be seen from the case studies, misalignment is especially effective on the camera-carrier inner gimbal wring. For this reason, this study added it only to the inner gimbal wring, and the misalignment in the outer gimbal wring was neglected.)

$$V = mgl(cos(\theta) - 1) \quad (2)$$

Torque is calculated from the Lagrangian equation by equation (3).

$$T_i = \frac{d}{dt}\frac{\partial L}{\partial \dot{\lambda}_i} - \frac{\partial L}{\partial \lambda_i} \quad (3)$$

In the equation, λ_i indicates the axis rotation amount, and $\dot{\lambda}_i$ indicates the axis angular velocity. Assuming no misalignment, equations (4) and (5) are found using equations (1), (2), and (3) [10]. The model of the dynamic equations is given in Figure 3.

$$T_\varphi = (J_{Kz} + J_{Iz})\left(\ddot{\varphi}\, sin^2(\theta) + 2\dot{\varphi}\dot{\theta}\, sin(\theta)\, cos(\theta)\right) + (J_{Kx} + J_{Ix})\left(\ddot{\varphi}\, cos^2(\theta) - 2\dot{\varphi}\dot{\theta}\, sin(\theta)\, cos(\theta)\right) + (J_{Dz})\ddot{\varphi} \quad (4)$$

$$T_\theta = (J_{Ky} + J_{Iy})\ddot{\theta} + (J_{Kx} + J_{Ix} - J_{Kz} - J_{Iz})\dot{\varphi}^2\, cos(\theta)\, sin(\theta) + mglsin(\theta) \quad (5)$$

3. DESIGNING OF STABILIZATION ALGORITHMS

Actuators drive the axes wrings of the gimbal with DC motors. Direct drive DC torque motors were used in the gimbal. Motors are mounted directly on both gimbal axes' wrings. The parameters of the motor are given in the appendix. The required stabilization command generates commands for the pitch and yaw axes. These commands are applied to the actuators separately from the control systems, and the gimbal stabilization is performed. The outputs of the gyro sensor are also given as feedback to the control systems [25]. The stabilization process is given in Figure 4. In this study, the cascade controller is designed to achieve more precise and robust control. Speed control is done with the PI controller in the inner loop. The outer loop is the stabilization loop and uses the angle information from the gyro sensor as feedback. The designs and tests made in this context are given in this study.

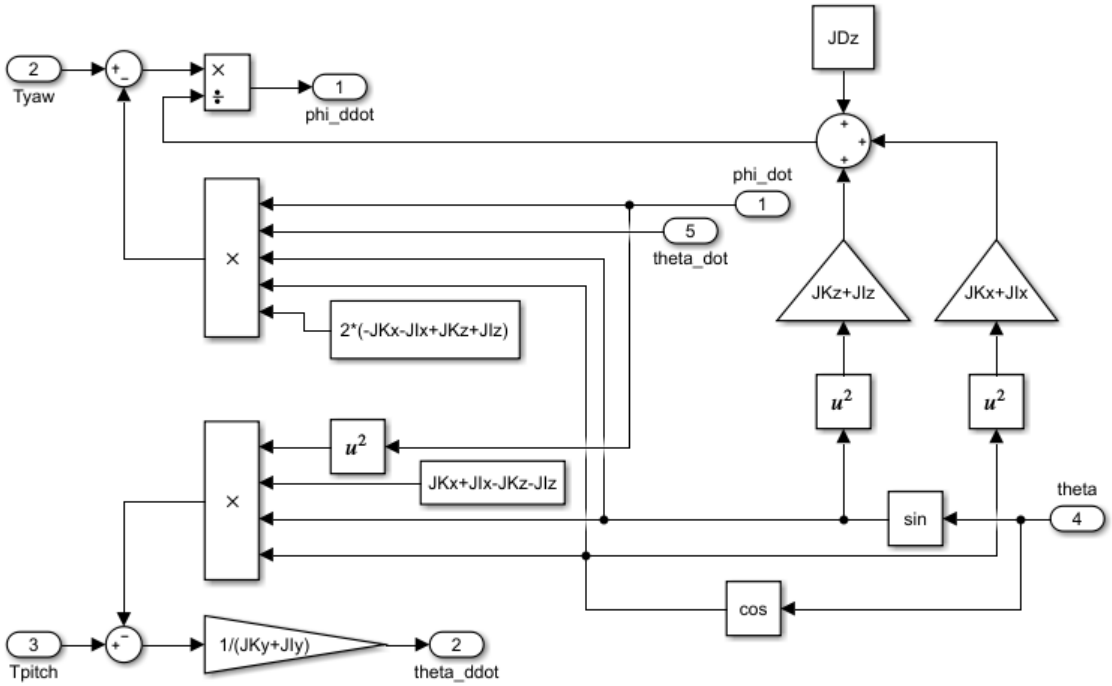

Figure 3. The model of the dynamic equations

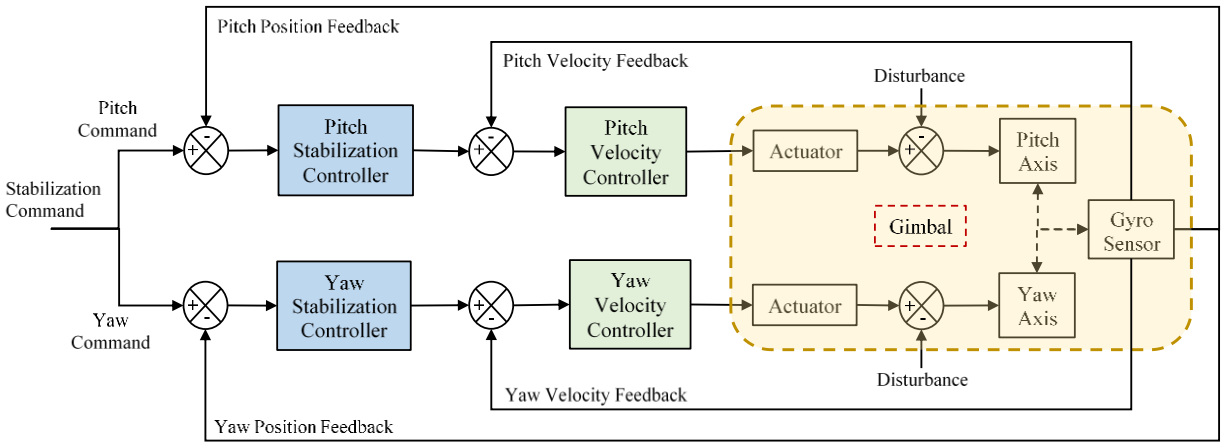

Figure 4. The stabilization process

3.1 Self-Tuning Fuzzy PID Control

Fuzzy PID control is realized using the error, the error's variation, and the error's integral at the controller input. This system has some disadvantages. Since the controller has three inputs, the number of rules to be created in the fuzzy controller structure is also very high. Also, it is difficult to follow the integral of the error by the controller and make adjustments in the process. The integral of the error has been removed from the control system to eliminate these disadvantages [26]. In this study, Self-Tuning Fuzzy PID (STF-PID) control method is designed, which analyzes the error and the derivative of the error and produces the necessary PID coefficients. Fuzzy logic consists of 3 main parts: fuzzifier, rules, and

defuzzifier. The inputs' membership functions and membership degrees are determined in the fuzzifier section. The rules section evaluates the fuzzy data under specific rules and produces the most appropriate output value. These data are fuzzy, so in the defuzzifier section, the output is evaluated with membership functions and brought into a structure that can be applied to the system [27]. The block diagram of the design is given in Figure 5.

The error and error's derivative are taken into the fuzzy logic controller and fuzzified with the input membership functions. The triangle membership function was used because it can be easily integrated into the application [27,28]. Input membership functions were defined in the range [-3, 3]. In order to increase the control sensitivity, seven states were defined within the scope of the input and output membership functions. These situations are given in Table 1, and the representation of the input membership function is given in Figure 6. Output membership functions are defined using the same method [0,100].

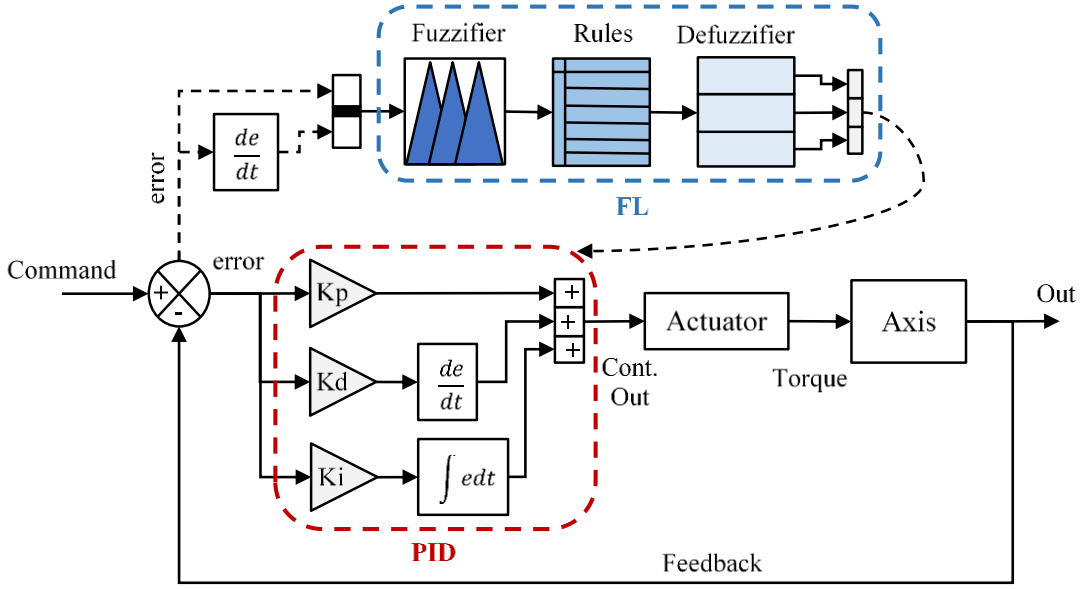

Figure 5. The block diagram of STF-PID

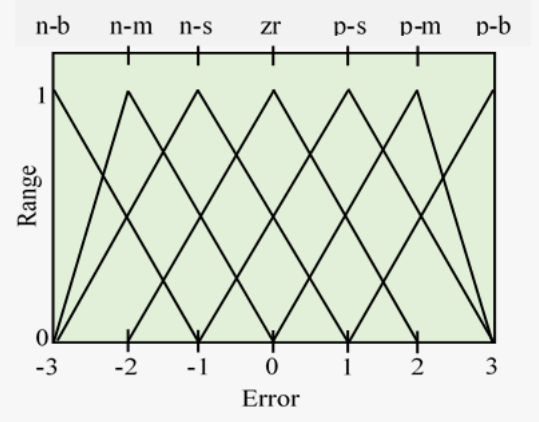

Figure 6. The input membership function

The rules section is prepared by considering the PID controller features, and Kp, Ki, and Kd values are obtained with these rules. While creating the rule tables, basic PID principles such as those given below were considered [29, 30].

- ✓ Where the error is large, choosing Kp as significant, Kd as small, and Ki as zero will prevent a significant overshoot [29, 30].
- ✓ When the error is moderate, Kp should be small, and Ki should be moderate. In this case, Kd is effective on the system. Finding the value of Kd, the derivative of the error is checked. If the derivative of the error is large, Kd should be small, and if the derivative of the error is small, Kd should be large [29, 30].
- ✓ When the error is small, the system response settles. In this case, Kp and Ki values should be large to protect the system against disturbance load and make it robust. Within the scope of the state of Kd, it is necessary to look at the derivative of the error. If the derivative of the error is large, Kd should be small, and if the derivative of the error is small, Kd should be large [29, 30].

Rule tables of Kp, Ki and Kd are given in Appendix. The Rules section has an inference mechanism along with the rule table. The inputs pass through the membership functions. After that, they are processed by the inference mechanism according to the rules defined as "if - else if - else". Mamdani method was used as the fuzzy inference mechanism [31].

Table 1. States of input membership functions

States	Sym	Range	States	Sym	Range
Negative big	n-b	{-3,-1,-1}	Positive small	p-s	{-1,1,3}
Negative middle	n-m	{-3,-2,-0}	Positive middle	p-m	{0,2,3}
Negative small	n-s	{-3,-1,1}	Positive big	p-b	{1,3,3}
Zero	zr	{-2,0,2}			

3.2 PSO Based PID Control

Particle Swarm Optimization (PSO) is a meta-heuristic method inspired by the behavior of swarms. It is also used successfully in multi-objective and nonlinear optimization problems. PSO is started with a group of random solutions, and updates are tried to find the optimum solution. At each iteration, the particle values are updated according to the particle best value (pbest) and global best value (gbest). Particle velocities and positions are updated according to the equations given below [32, 33].

$$v_i^{k+1} = v_i^k + c_1 * rand_1^k * \left(pbest_i^k - x_i^k\right) + c_2 * rand_2^k * \left(gbest^k - x_i^k\right) \quad (8)$$

$$x_i^{k+1} = x_i^k + v_i^{k+1} \quad (9)$$

$$Kp_i^{k+1} = Kp_i^k + c_1 * rand_1^k * \left(pbest_i^k - Kp_i^k\right) + c_2 * rand_2^k * \left(gbest^k - Kp_i^k\right) \quad (10)$$

$$Ki_i^{k+1} = Ki_i^k + c_1 * rand_1^k * \left(pbest_i^k - Ki_i^k\right) + c_2 * rand_2^k * \left(gbest^k - Ki_i^k\right) \quad (11)$$

$$Kd_i^{k+1} = Kd_i^k + c_1 * rand_1^k * \left(pbest_i^k - Kd_i^k\right) + c_2 * rand_2^k * \left(gbest^k - Kd_i^k\right) \quad (12)$$

The c_1 and c_2 parameters are learning factors. c1 causes the particle to act according to its own experience, and c2 causes the particle to behave according to the experiences of other particles in the swarm. The $rand_1^k$ and $rand_2^k$ in the equation are random numbers with a uniform distribution between [0, 1]. *k* is the iterations' number, and *i* is the particle index. Using (8) and (9), the equations below were prepared to calculate the PID coefficients.

The c1 and c2 parameters have a direct effect on the behavior of the particles. The particles move at constant speeds if c1 and c2 are both 0. If c1>0 and c2=0, the particles do not follow the global best and act individually. If c2>0 and c1=0, the particles move only according to the global best. Under these conditions, the equality of c1 and c2 can not dominate the local and global sections [34].

The integral of the absolute value of the error is generally used as the objective function for control systems optimization. Operating with only the error value causes the controller output to increase sharply due to the integral, especially when the error is large. This situation can cause overshoot and even oscillation in the system response. Therefore, the controller output is used with the error in the objective function, given in equation (13).

$$J = \int_0^\infty |e(t)|dt + \int_0^\infty |CO(t)|dt \quad (13)$$

The block diagram of PSO-PID is given in Figure 7. This section is integrated into the FL location in Figure 3.

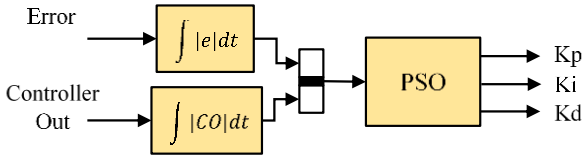

Figure 7. The block diagram of PSO-PID

Simulations were carried out with different particle numbers (5-20) and iterations (10-100) for optimization studies with PSO. (Algorithm parameters are given in the Appendix.) Simulation studies started with five particles and ten iterations, increasing these numbers for the system responses to reach the desired level. In the simulation, a 1-degree step command was applied to the axes. There was no significant difference between 50 and 100 iterations in 20-particle trials. For this reason, the population number was determined as 20 and iteration 50. The PID coefficients and the cost found as a result of each optimization are given in Table 2. System responses for six different optimizations are given in Figure 8.

Table 2. PID coefficients

Opt.	Particle	Iteration	Pitch Axis				Yaw Axis			
			Kp	Ki	Kd	Cost	Kp	Ki	Kd	Cost
PSO1	5	10	54.5	74.2	0.36	0.072	32.1	24.8	0.67	0.071
PSO2	5	20	41.8	62.5	0.38	0.070	34.7	34.3	0.35	0.068

PSO3	10	20	31.7	58.1	0.36	0.068	34.1	44.2	0.39	0.065
PSO4	10	50	26.4	41.1	0.24	0.066	30.9	41.4	0.32	0.064
PSO5	20	50	26	41.6	0.13	0.065	30.8	41.1	0.40	0.063
PSO6	20	100	26.1	41.8	0.14	0.065	30.7	41.1	0.34	0.063

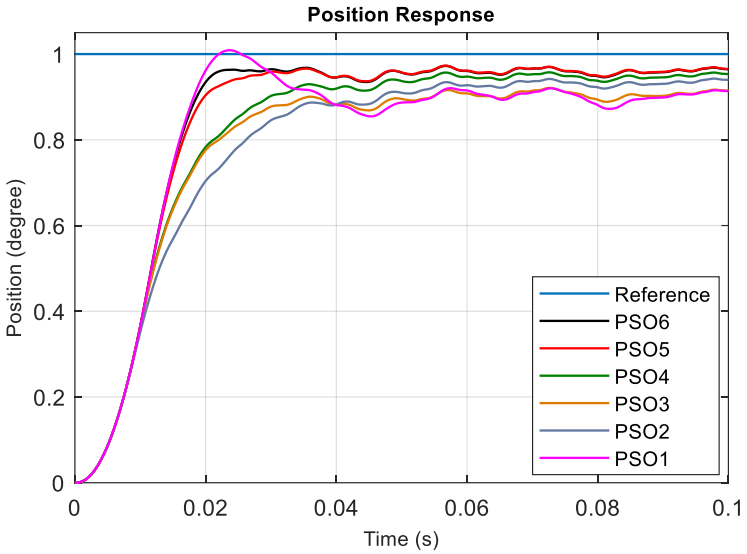

Figure 8. Optimization results

4. EXPERIMENTAL TESTS AND RESULTS

A compact RIO (Reconfigurable Input Output) based real-time test system was used within the algorithm test scope. The stabilization algorithm and the data taken from the gimbal system are on the compact RIO. The stabilization angles are transmitted to the gimbal system by the host computer. In addition, a three-axis Stewart platform is used to simulate missile flight. Figure 9 shows the view of the test system [23].

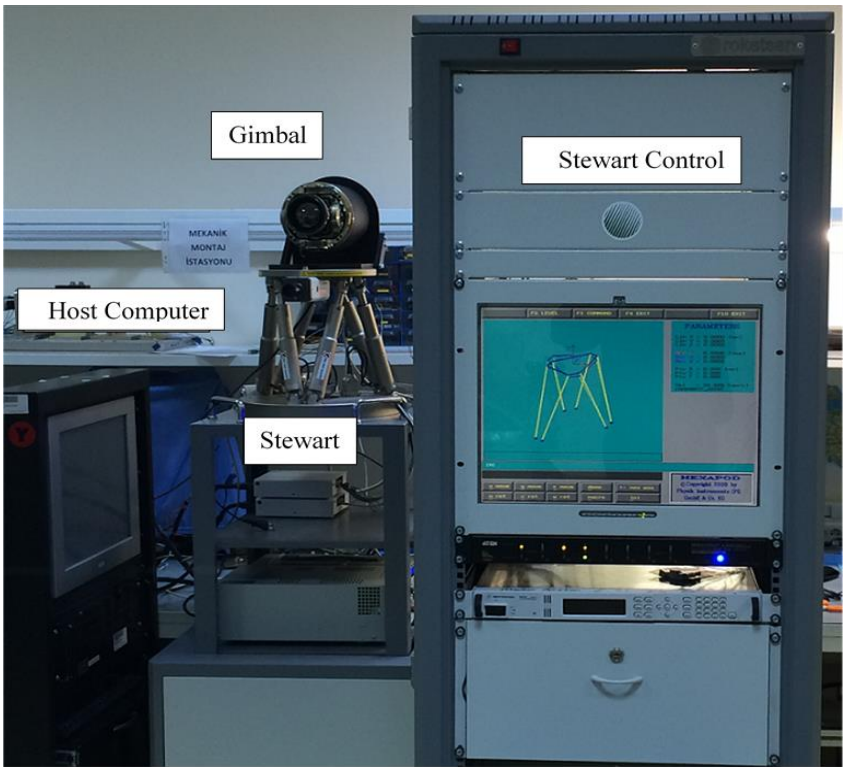

Figure 9. Test system

Within the scope of the tests, first, the motion control of the axes was carried out without operating the Stewart Platform. In this context, square wave and ramp reference commands were applied to the pitch and yaw axes.

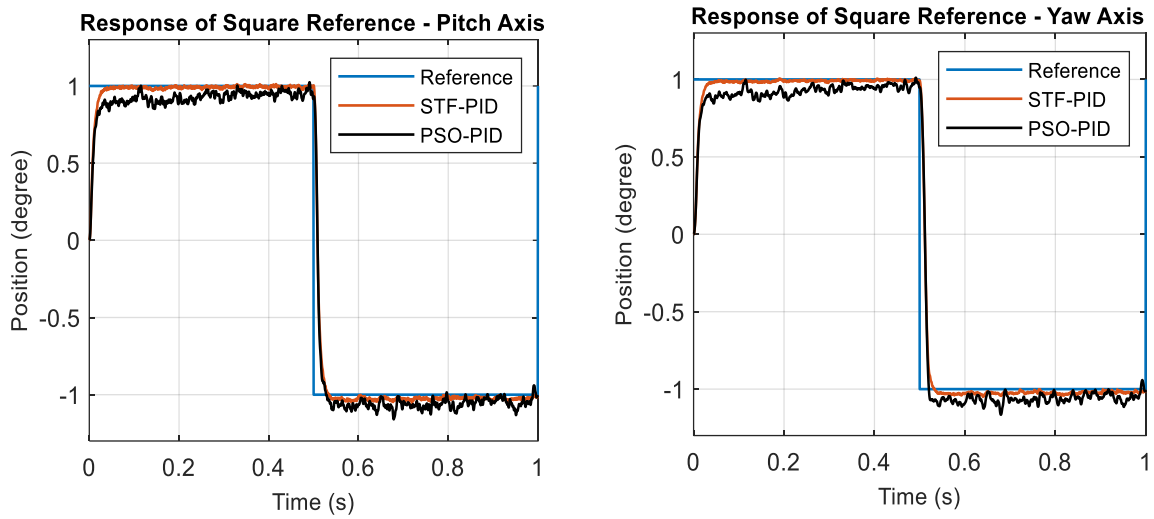

Figure 10. Responses to square references

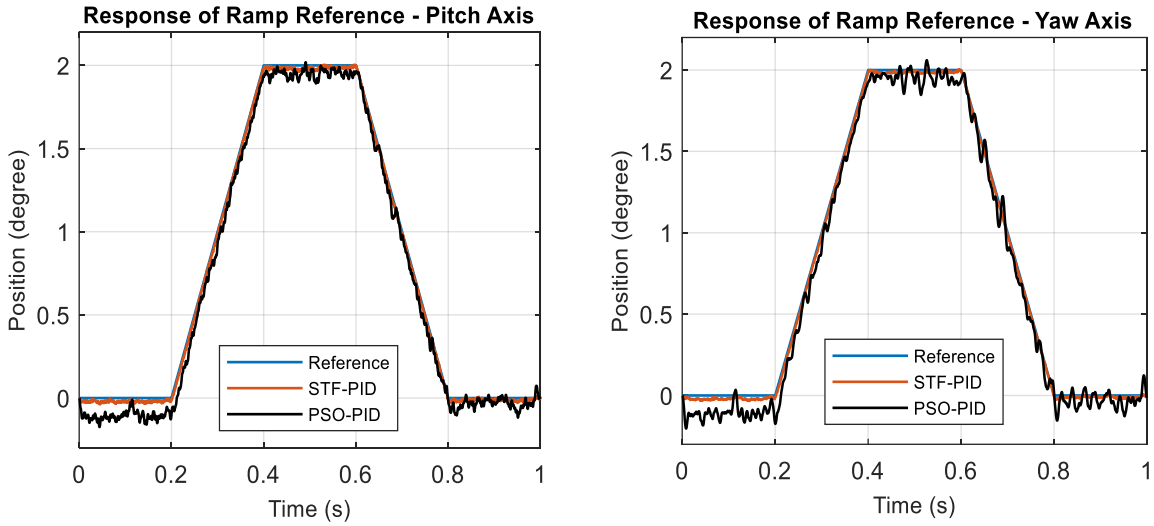

Figure 11. Responses to ramp references

Figures 10 and 11 show the responses of the axes to the square and ramp reference. As can be seen from the graphs, the rise times of both controllers are pretty enough for control (Rise times were 16.5 ms with STF-PID and 26 ms with PSO-PID.). They were able to respond quickly to the requested reference. The main difference is seen at the time of the settling zone. No external load was applied to the gimbal in this test. However, sensors on the gimbal, wiring, mechanical frictions, and eccentricities already create a load. The error and the error's derivative are evaluated in each cycle with the STF-PID controller, and the PID coefficients are set to the appropriate levels. This feature increases the robustness of the controller's system response when the error is large and reduces the overshoot and steady-state error in the system response by lowering the coefficients when the error is small. The coefficient changes in the square reference test are given in Figure 12.

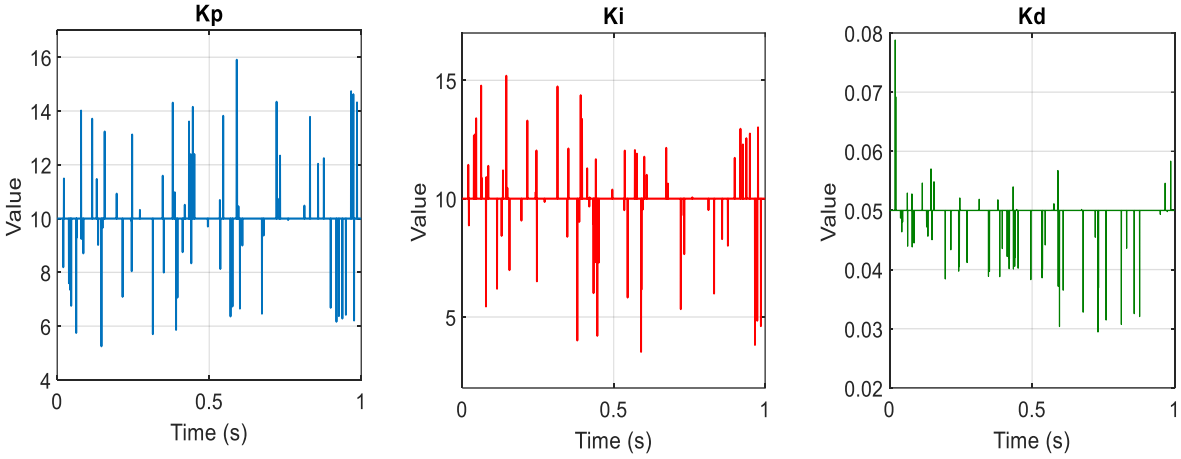

Figure 12. PID coefficients

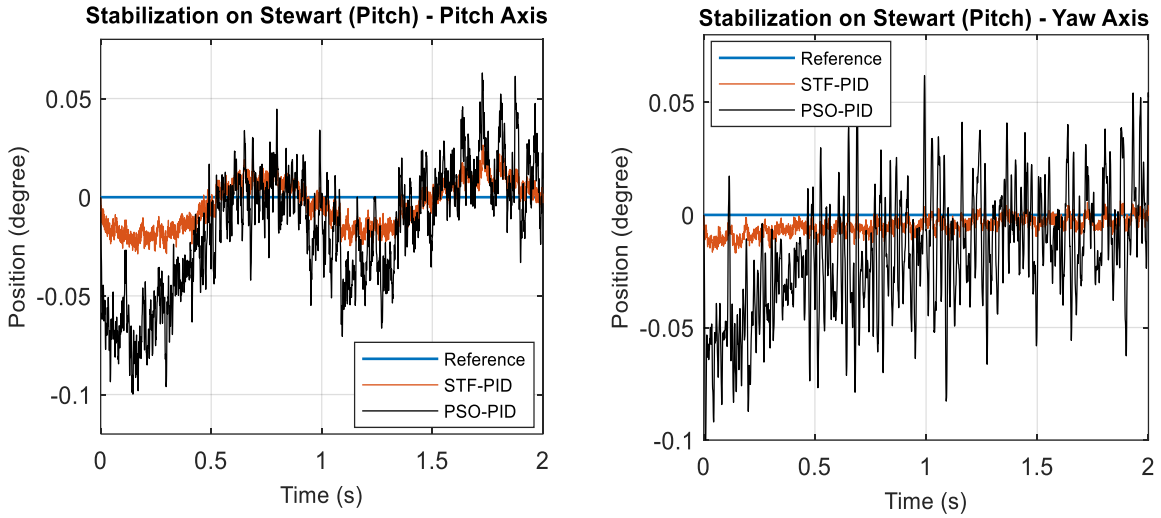

Figure 13. Tests on the pitch axis

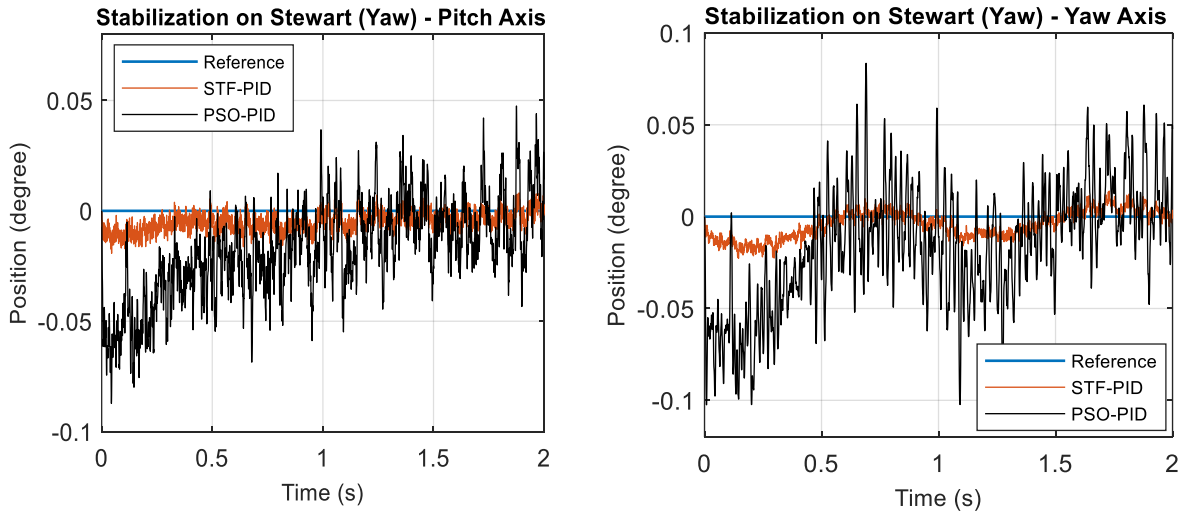

Figure 14. Tests on the yaw axis

In the second part of the experimental studies, 10 degrees 1 Hz sinusoidal disturbance effects were given to the gimbal on the pitch and yaw axes with the Stewart platform. The graphs of the results of the tests are given

in Figures 13 and 14. In the tests performed with Stewart, stabilization was performed with the STF-PID controller with errors of 20-30E-3 degrees. In the tests performed with the PSO-PID controller, the error values were up to 50-80E-3 degrees. Against external load, STF-PID reduced the error by parameter setting, as in previous tests. It is seen that the error values in the pitch axis (30E-3 degrees) with STF-PID are higher than the yaw axis (20E-3 degrees). It is estimated that the inertia and mechanical friction values of the pitch axis on which the camera is carried are higher than the values of the yaw axis. These differences affected the DC motor controlling the pitch axis as more load and caused the stabilization error to be higher in this axis.

PID coefficient changes of pitch axis tests are given in Figure 15. PID coefficients obtained with PSO are also shown in the Figure. The variation of the coefficients in STF is also seen here.

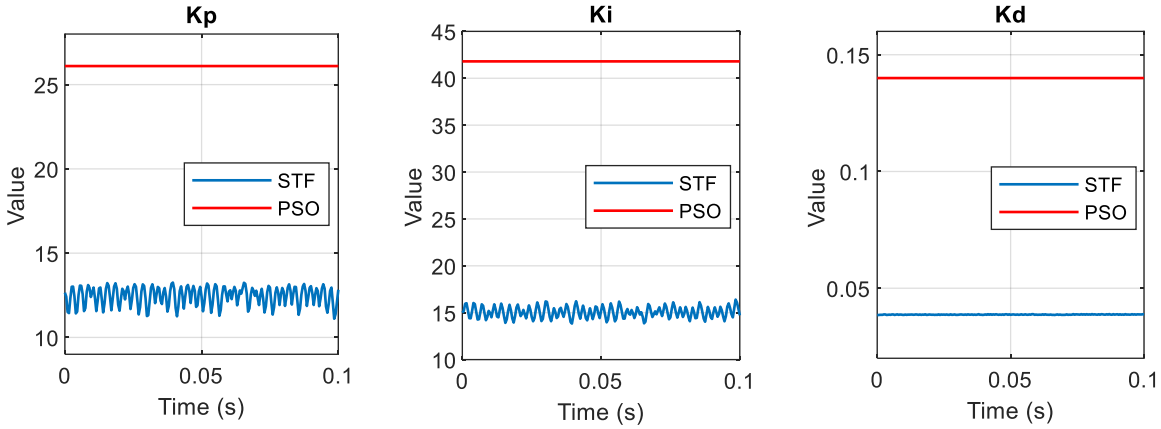

Figure 15. PID coefficients changes

5. CONCLUSION

This study carried out controller design and implementation studies within the scope of stabilization of a two-axis gimbal system used in the missile. Different loads may fall on the axes in the gimbal due to cable stiffness, mechanical friction, and axial misalignment. With the STF-PID designed in this context, the PID coefficients were adjusted differently at each step, and a more efficient controller was obtained. In the tests performed with the Stewart platform, stabilization errors of 20E-3 degrees were reached. Error-values exceeded 50E-3 degrees with the controller designed with PSO, which is an effective optimization method. This situation indicates that the adjustable PID controller is more suitable than the fixed coefficient PID controller for the gimbal with uncertainties.

ACKNOWLEDGEMENTS

The author would like to thank Roketsan Inc. for their financial support for this work.

DECLARATION OF ETHICAL STANDARDS

The author of this article declare that the materials and methods used in this study do not require ethical committee permission and/or legal-special permission.

AUTHORS' CONTRIBUTIONS

Murat ŞAHİN: Did the literature review and designed the control systems. Performed experiments and analyzed the results. Wrote the manuscript.

CONFLICT OF INTEREST

There is no conflict of interest in this study.

REFERENCES

[1] Ahmed, F., Mohanta, J. C., Keshari, A., and Yadav, P. S., "Recent Advances in Unmanned Aerial Vehicles: A Review", ***Arabian Journal for Science and Engineering***, 47(7): 7963-7984, (2022).

[2] Toloei, A. R., Pirzadeh, M., and Vali, A. R., "Design of predictive control and evaluate the effects of flight dynamics on performance of one axis gimbal system, considering disturbance torques", ***Aerospace Science and Technology***, 54: 143-150, (2016).

[3] Cong Danh, N., "The Stability of a Two-Axis Gimbal System for the Camera", ***The Scientific World Journal***, 1-8, (2021).

[4] Khayatian, M., and Arefi, M. M., "Adaptive dynamic surface control of a two-axis gimbal system", ***IET Science, Measurement & Technology***, 10(6): 607-613, (2016).

[5] Lee, D. H., Tran, D. Q., Kim, Y. B., and Chakir, S., "A robust double active control system design for disturbance suppression of a two-axis gimbal system", ***Electronics***, 9(10): 1638, (2020).

[6] Yang, H., Zhao, Y., Li, M., and Wu, F., "The static unbalance analysis and its measurement system for gimbals axes of an inertial stabilization platform", ***Metrology and measurement systems***, 22(1): 51-68, (2015).

[7] Wen, T., Xiang, B., and Wong, W., "Coupling analysis and cross-feedback control of three-axis inertially stabilized

platform with an active magnetic bearing system", ***Shock and Vibration***, 1-17, (2020).

[8] Tong, W., Xiang, B., and Wong, W., "Gimbal torque and coupling torque of six degrees of freedom magnetically suspended yaw gimbal", ***International Journal of Mechanical Sciences***, 168, 105312, (2020).

[9] Baskin, M., and Leblebicioğlu, M. K., "Robust control for line-of-sight stabilization of a two-axis gimbal system", ***Turkish Journal of Electrical Engineering and Computer Sciences***, 25(5): 3839-3853, (2017).

[10] Hasturk, O., Erkmen, A. M., and Erkmen, I., "Proxy-based sliding mode stabilization of a two-axis gimbaled platform", ***Target***, 3(4): 1-7, (2011).

[11] Naderolasli, A., and Tabatabaei, M., "Stabilization of the two-axis gimbal system based on an adaptive fractional-order sliding-mode controller", ***IETE Journal of Research***, 63(1): 124-133, (2017).

[12] Mousavi, Y., Zarei, A., and Jahromi, Z. S., "Robust adaptive fractional-order nonsingular terminal sliding mode stabilization of three-axis gimbal platforms", ***ISA transactions***, 123: 98-109, (2022).

[13] Mao, J., Li, S., Li, Q., and Yang, J., "Design and implementation of continuous finite-time sliding mode control for 2-DOF inertially stabilized platform subject to multiple disturbances", ***ISA transactions***, 84: 214-224, (2019).

[14] Sasaki, T., Shimomura, T., Pullen, S., and Schaub, H., "Attitude and vibration control with double-gimbal variable-speed control moment gyros", ***Acta Astronautica***, 152: 740-751, (2018).

[15] Ashok Kumar, M., and Kanthalakshmi, S., "H∞ Control law for line of sight stabilization in two-axis gimbal system", ***Journal of Vibration and Control***, 28(1-2): 182-191, (2022).

[16] Altan, A., and Hacıoğlu, R., "Model predictive control of three-axis gimbal system mounted on UAV for real-time target tracking under external disturbances", ***Mechanical Systems and Signal Processing***, 138, 106548, (2020).

[17] Jahanandish, R., Khosravifard, A., and Vatankhah, R., "Determination of uncertain parameters of a two-axis gimbal and motion tracking via Fuzzy logic control approach", ***Journal of Intelligent & Fuzzy Systems***, 39(5): 6565-6577, (2020).

[18] Abdo, M. M., Vali, A. R., Toloei, A. R., and Arvan, M. R., "Stabilization loop of a two axes gimbal system using self-tuning PID type fuzzy controller", ***ISA transactions***, 53(2), 591-602, (2014).

[19] Danh, N. C., "LQG, PID controller, ANN for single axis gimbal actuator", ***EAI Endorsed Transactions on AI and Robotics***, 1(1): 1-11, (2022).

[20] Sharma, J., Hote, Y. V., and Prasad, R., "Robust PID control of single-axis gimbal actuator via stability boundary locus", ***IFAC-PapersOnLine***, 53(1): 27-32, (2020).

[21] Senthil Kumar, S., and Anitha, G., "Fuzzy Logic-Based Self-Tuning PID Controllers Using Parameters Adaptive Method for Stabilization of a Two-Axis Seeker Gimbal", ***IETE Journal of Research***, 1-10, (2021).

[22] Srivastava, A.K., Kumar, D., Tripathi, S.M. and Sen, P.K., "Comparative study of proportional-integral and proportional-integral-derivative (PI and PID) controllers for Z-source inverter-fed induction motor drive", ***2nd International Conference on Power, Control and Embedded Systems (ICPCES)***, Allahabad, India, 1-6, (2012).

[23] Sahin, M., "Kendinden ayarlamalı PID kontrolör ile iki eksenli gimbal uygulaması", ***PhD Thesis***, Gazi University, Graduate School of Natural and Applied Sciences, (2015).

[24] Hemingway, E. G., and O'Reilly, O. M., "Perspectives on Euler angle singularities, gimbal lock, and the orthogonality of applied forces and applied moments", ***Multibody System Dynamics***, 44(1): 31-56, (2018).

[25] Senthil Kumar, S., and Anitha, G., "A novel self-tuning fuzzy logic-based PID controllers for two-axis gimbal stabilization in a missile seeker", ***International Journal of Aerospace Engineering***, 1-12, (2021).

[26] El-Samahy, A. A., and Shamseldin, M. A., "Brushless DC motor tracking control using self-tuning fuzzy PID control and model reference adaptive control", ***Ain Shams Engineering Journal***, 9(3): 341-352, (2018).

[27] Aissaoui, A. G., and Tahour, A., "Application of Fuzzy Logic in Control of Electrical Machines", ***Fuzzy Logic – Controls, Concepts, Theories and Applications***, 107-129, (2012).

[28] Tüzüner, Z., and Bal, H., "Three Group Classification Problem Approach Based on Fuzzy Goal Programming", ***Politeknik Dergisi***, 23(4): 1089-1095, (2020).

[29] Xue, P., Wang, H., Hou, J., and Li, W., "Based on the Fuzzy PID Brushless DC Motor Control System Design", ***International Conference on Measurement, Information and Control***, 703-706, (2012).

[30] Pedrammehr, S., Qazani, M. R. C., Asadi, H., Ettefagh, M. M., and Nahavandi, S., "Model-based control of axisymmetric hexarot parallel manipulators", ***Results in Control and Optimization***, 7, 100135, (2022).

[31] Pourjavad, E., and Mayorga, R. V., "A comparative study and measuring performance of manufacturing systems with Mamdani fuzzy inference system", ***Journal of Intelligent Manufacturing***, 30(3): 1085-1097, (2019).

[32] Dereli, S., Köker, R., Öylek, İ., and Mükremin, A. Y., "A comprehensive research on the use of swarm algorithms in the inverse kinematics solution", ***Politeknik Dergisi***, 22(1): 75-79, (2019).

[33] Tefek, M. F., "Küresel Optimizasyon Problemlerinin Çözümü İçin Zamanla Değişen Rastgele Atalet Ağırlıklı Jaya Algoritması", ***Politeknik Dergisi***, 25(1): 123-135, (2022).

[34] Kaveh, A., "Particle swarm optimization", ***In Advances in Metaheuristic Algorithms for Optimal Design of Structures***, 11-43, (2017).

APPENDIX

Table 3. Rules table of Kp

e/e'	*n-b*	*n-m*	*n-s*	*zr*	*p-s*	*p-m*	*p-b*
p-b	zr	zr	n-m	n-m	n-b	n-b	n-b
p-m	p-s	zr	n-s	n-m	n-m	n-m	n-b
p-s	p-s	p-s	zr	n-s	n-s	n-m	n-m
zr	p-s	p-m	p-s	zr	n-s	n-m	n-m
n-s	p-m	p-m	p-s	p-s	zr	n-s	n-s
n-m	p-b	p-b	p-m	p-s	p-s	zr	n-s
n-b	p-b	p-b	p-m	p-m	p-s	zr	zr

Table 4. Rules table of Ki

e/e'	*n-b*	*n-m*	*n-s*	*zr*	*p-s*	*p-m*	*p-b*
p-b	zr	zr	p-s	p-b	p-m	p-b	p-b
p-m	zr	zr	p-s	p-s	p-m	p-b	p-b
p-s	n-s	n-s	zr	p-s	p-s	p-m	p-m
zr	n-m	n-m	n-s	zr	p-s	p-m	p-m
n-s	n-m	n-b	n-s	n-s	zr	p-s	p-s
n-m	n-b	n-b	n-s	n-s	n-s	zr	zr
n-b	n-b	n-b	n-m	n-m	n-s	zr	Zr

Table 5. Rules table of Kd

e/e'	*n-b*	*n-m*	*n-s*	*zr*	*p-s*	*p-m*	*p-b*
p-b	p-b	p-m	p-m	p-m	p-s	p-s	p-b
p-m	p-b	p-s	p-s	p-s	p-s	p-s	p-m
p-s	zr	zr	zr	zr	zr	zr	zr
zr	zr	n-s	n-s	n-s	n-s	n-s	zr
n-s	zr	n-s	n-m	n-m	n-s	n-s	zr
n-m	p-s	n-s	n-b	n-m	n-m	n-s	zr
n-b	p-s	n-m	n-b	n-m	n-b	n-m	p-s

Table 6. Parameters of PSO

Parameter	**Value**
nParticle	5 – 20
nIterations	10 – 100
Particle_min	0
Particle_max	100
cognitiveConstant (c1)	2
socialConstant (c2)	2

Table 7. Parameters of DC Motor

Parameter	**Value**
Inertia (J_m)	$2.8\ g.cm^2$
Torque constant (K_t)	$21.2\ mN.m/A$
Resistance (R)	$7\ \Omega$
Inductance (L)	$5\ mH$
Voltage constant (K_e)	$0.021\ {}^{V}/_{rad/s}$